Naunyn-Schmiedeberg's Archives of Pharmacology (2023) 396:1797–1810
https://doi.org/10.1007/s00210-023-02433-5

RESEARCH

Synthesis and bioassay of 3-Aryl -1-(pyridin-4-yl)benzo[4,5] imidazo[1,2-*d*][1,2,4]- triazin-4(3*H*)-ones as anti-cancer agents

Bassam Abu Thaher[1] · Ihab Al-Masri[2] · Kanan Wahedy[2] · Rami Morjan[1] · Saeb Aliwaini[3] · Iman Mahmoud Al atter[3] · Aayat Ahmed Elmabhouh[3] · Areej khaled AL ibwaini[3] · Saba Luay Alkhaldi[3] · Basem Qeshta[1] · Claus Jacob[4] · Hans-Peter Deigner[5,6]

Received: 3 November 2022 / Accepted: 16 February 2023 / Published online: 1 March 2023

Abstract

Four novel 3-Aryl -1-(pyridin-4-yl)benzo[4,5]imidazo[1,2-*d*][1,2,4]- triazin-4(*3H*)-ones derivatives (C1 to C4) have been designed, synthesized, and evaluated for their anticancer activity. The structure of compounds was characterized by IR, ^{1}H NMR, ^{13}C NMR and high-resolution mass (HRMS). The crystal structures of C1, C2 and C4 were previously determined by single-crystal X-ray analysis.

The results from docking experiments with EGFR suggested the binding of the compounds at the active site of EGFR. The new compounds exhibited different levels of cytotoxicity against HCC1937 and MCF7 breast cancer cells. Results of the MTT assay identified C3 as the most cytotoxic of the series against both MCF7 and HCC1937 breast cancer cell lines with IC_{50} values of 36.4 and 48.2 μM, respectively. In addition to its ability to inhibit cell growth and colony formation ability, C3 also inhibited breast cancer cell migration. Western blotting results showed that C3 treatment inhibited EGFR signaling and induced cell cycle arrest and apoptosis as indicated by the low level of p-EGFR and p-AKT and the increasing levels of p53, p21 and cleaved PARP. Our work represents a promising starting point for the development of a new series of compounds targeting cancer cells.

Keywords Aryl · Pyridine · Benzoimidazole · [1,2,4]triazinone · EGFR · Breast cancer · Docking

Introduction

Cancer is still the second leading cause of death and is responsible for the majority of human deaths. Generally, there have been continuous efforts against cancer with a lot of achievements in the treatment and diagnosis strategies. However, successful treatment is yet to be achieved. One strategy to develop new anticancer therapeutic agents is molecular hybridization which depends on the combination of two or more biologically active molecules in one structure, which by synergistic effects between them, could provide improved therapeutic agents (Krause et al. 2017; Guo and Diao 2020; Sivaramakarthikeyan et al. 2020). In addition; hybrid molecules may enhance the therapeutic effects and improve specificity as well as could beat drug resistance. Different chemotherapeutic agents synthesized through molecular hybridization strategy are now commercially available and many others are still at different phases of clinical trials. For example; Avapritinib and Capmatinib

✉ Saeb Aliwaini
siwini@iugaza.edu.ps; saib.iwini@gmail.com

✉ Hans-Peter Deigner
Hans-Peter.Deigner@hs-furtwangen.de

1 Faculty of Science, Chemistry Department, Islamic University of Gaza, P.O. Box 108, Gaza, Palestine

2 Faculty of Pharmacy, Al-Azhar University, Gaza, Palestine

3 Department of Biology and Biotechnology, Islamic University of Gaza, PO Box 108, Gaza, Palestine

4 Division of Bioorganic Chemistry, School of Pharmacy, Saarland University, D-66123 Saarbruecken, Germany

5 Faculty of Medical and Life Sciences, Hochschule Furtwangen (HFU), Jakob-Kienzle-Strasse 17, 78054 Villingen-Schwenningen, Germany

6 Fraunhofer IZI, Perlickstrasse 1, 04103 Leipzig, Germany

have been approved by the FDA as potential therapeutic options. (Fig. 1) (Kayki et al. 2022).

Triazines are heterocyclic aromatic compounds containing three nitrogen atoms in their frame. They exist in three known isomeric structures namely; 1,2,3-triazine, 1,2,4-triazine, and 1,3,5-triazine. Their systematic names are based on the relative positions of the nitrogen atoms within the six-membered ring (Kushwaha and Sharma 2020). Triazines exhibit potential antitumor effects through their ability to interact with several targets in cancer cells and interfering with important signaling pathways to induce cell cycle arrest and apoptosis (Peterson et al. 2011; Singla et al. 2015; Yuan et al. 2019; Schuler et al. 2020; Majeed Ganai et al. 2021; Hashem et al. 2022). For example, 1,2,4-triazine and benzimidazole derivatives have attracted interest for their efficacy in preventing and treating cancer at different stages of the disease progression, and their anticancer activity has been widely reported. Recent reports showed that Triazine hybrids could interfere with various signaling pathways to induce cancer cell death (Hashem et al. 2022). Different subfamilies of 1,2,4-triazines, including 5,6-diaryl- 1,2,4-triazines have also been prepared and tested against different cancer cell lines recently (Singla et al. 2015; Abu Thaher et al. 2016a; Sahin et al. 2022). Some of them showed potent anti-proliferative and anti-migration effects against violent cancer cell lines. On the other hand, compounds containing a benzimidazole core have been tackled in the area of pharmaceuticals (Wahedy et al. 2017). Important reports showed that several benzimidazole-based compounds have anti-tumor activity against a panel of human cancer cell lines (Thomas et al. 2007; Gellis et al. 2008; Refaat 2010; Akhtar et al. 2018a, b; Gaber et al. 2018; Celik et al. 2019; Yuan et al. 2019; Nawaz et al. 2020; Sivaramakarthikeyan et al. 2020; AboulWafa et al. 2020; Sharma et al. 2021; Sherbiny et al. 2021; Hashem et al. 2022). Interestingly, triazine benzimidazole compounds have also been synthesized and tested as inhibitors of important cellular pathways such as EGFR, PI3K and MET pathways (Peterson et al. 2011; Schuler et al. 2020; Choi et al. 2021; Hashem et al. 2022). Some of these compounds induced potent antiproliferative effects by inhibiting EGFR and down-regulating the oncogenic parameter p53 ubiquitination (Hashem et al. 2022). It is worth mentioning that EGFR tyrosine kinase is the most important target for breast and lung cancer treatments due to its roles in tumor initiation and progression by regulating cell growth, differentiation, migration, and apoptosis (Sahin et al. 2022; Zhang et al. 2022; Tan et al. 2022).

Taking into account all of the above-mentioned facts, we hypothesized that the combination of 1,2,4-triazine and benzimidazole scaffold in the same molecule could lead to novel analogs with increased antitumor efficacy as compared to their parent triazine. In this regard, four new Benzoimidazo[1,2,4] triazinones have been designed, prepared, characterized, and evaluated against breast cancer cells.

Materials and methods

General procedure for the synthesis of hydrazones (iiia-d)

0.11 mol of aryl hydrazine was dissolved in 80 mL glacial acetic acid, and 0.1 mol of 4-pyridincarboxaldehyde was

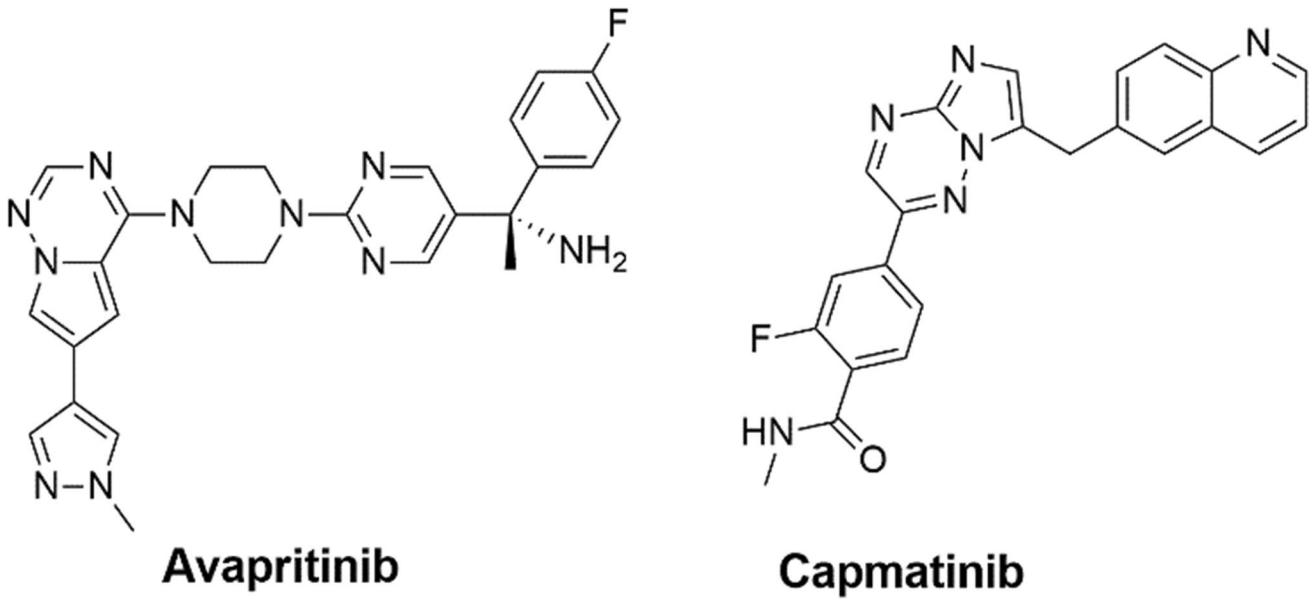

Fig. 1 Representative therapeutic agents approved by the FDA

added to the reaction mixture and was stirred at room temperature until the reaction was finished (as monitored by TLC). A pale yellow solid was collected by filtration and washed with water, EtOH, and petroleum ether. The preparation of all hydrazones was made following previously established protocols (Abu Thaher et al. 2012a, b, c, 2016b; Aliwaini et al. 2021a).

General procedure for the synthesis of hydrazonyl chlorides (iva-d)

0.011 mol of the corresponding hydrazone was dissolved in a minimum amount of dry DMF (4 mL) at room temperature, 0.012 mol of *N*-chlorosuccinimide (NCS) was added portion-wise to the reaction. The reaction became hot and then the product was precipitated suddenly, and the reaction was finished (by TLC). The solid was collected by filtration and washed with petroleum ether. The preparation of all hydrazonyl chlorides was made following established protocols (Thaher et al. 2012; Abu Thaher et al. 2012a, b, c; Burnet et al. 2016; Abu Thaher et al. 2016b; Aliwaini et al. 2021a).

General procedure for the synthesis of the target compounds C1 to C4

2.1 mmol (50.4 mg) of NaH was added slowly to a solution of 2.1 mmol (390 mg) of ethyl-2- benzimidazolcarboxylate v in 30mL dry THF and continued stirring at RT for about 20 minutes. Then, 2.0 mmol of the corresponding pyridinecarbohydrazonoyl chloride Iva-d was added slowly portion-wise to the reaction mixture and in parallel 0.5 mL of Et_3N was added drop-wise. The reaction was left stirring overnight, and it was controlled by TLC until it was finished. The reaction was filtered and concentrated under a vacuum. The solid residue was purified by column chromatography (heptane: ethyl acetate; 2:1, then 1:1).

C1: 3-(2,4,6-trichlorophenyl)-1-(pyridin-4-yl)benzo[4,5] imidazo[1,2-d][1,2,4]triazin-4(3H)-one

Colorless plates were obtained from the slow evaporation of a hexane/ ethyl acetate solution. Yield: 178 mg, 20% mp 254-255 °C; ^{1}H NMR (400 MHz, DMSO-*d*6) δ 8.92 (d, J = 5.8 Hz, 2H, pyridine), 8.09 (d, J = 8.2 Hz, 1H, benzimidazole), 8.01 (s, 2H, trichlorophenyl), 7.85 (d, , J = 5.9 Hz, 2H, pyridine), 7.60 (t, J = 7.7 Hz, 1H, benzimidazole), 7.44 (t, J = 7.9 Hz, 1H, benzimidazole), 6.69 (d, J = 8.5 Hz, 1Hm benzimidazole). ^{13}C NMR (100 MHz, DMSO) δ 151.72, 151.12, 143.91, 140.41, 138.29, 137.42, 136.34, 134.87, 134.38, 129.58, 129.44, 127.08, 127.02, 124.20, 122.30, 114.50. IR: 3051 (CH aromatic),1693, 1610 (CON, C=N), 1595, 1509 (aromatic rings), 1444, 1405, 1328, 1287, 1266, 1147, 994, 840, 809, 740 cm^{-1}; EI-HRMS *m/z* calcd. for $C_{20}H_{10}Cl_3N_5ONa$: [M+Na] = 463.98474 found 463.98431.

C2: 3-(4-bromophenyl)-1-(pyridin-4-yl)benzo[4,5] imidazo[1,2-d][1,2,4]triazin-4(3H)-one

Colorless plates were obtained from the slow evaporation of a hexane/ ethyl acetate solution. Yield: 209 mg, 25%;; mp 302-303 °C; ^{1}H NMR (400 MHz, DMSO-*d*6) δ 8.94 (d, J = 5.5 Hz, 2H, pyridine), 8.04 (d, J = 8.0 Hz, 1H, benzimidazole), 7.84 (d, J = 5.2 Hz, 2H, pyridine), 7.75 (d, J = 8.8 Hz, 2H, p-bromobenzene), 7.70 (d, J = 8.8 Hz, 2H, p-bromobenzene), 7.55 (t, J = 7.9 Hz, 1H, benzimidazole), 7.38 (t, J = 7.8 Hz, 1H, benzimidazole), 6.65 (d, J = 8.6 Hz, 1H, benzimidazole). ^{13}C NMR (100 MHz, DMSO) δ 152.46, 151.15, 144.03, 141.61, 139.81, 138.05, 136.62, 132.84, 132.19, 132.01, 129.08, 127.83, 126.79, 126.72, 126.62, 126.45, 124.11, 122.20, 122.11, 121.07, 114.31, 114.14, 40.65, 40.44, 40.24, 40.03, 39.82, 39.61, 39.40. IR 3020 (CH aromatic), 1697, 1620 (CON, C=N), 1600, 1515 (aromatic rings), 1450, 1410, 1320, 1280, 1250, 1140, 990, 820, 737cm^{-1}; EI-HRMS *m/z* calcd. for $C_{20}H_{12}BrN_5ONa$: [M+Na] = 440.01226 found 440.01174.

C3: 3-(3,5-dichlorophenyl)-1-(pyridin-4-yl)benzo[4,5] imidazo[1,2-d][1,2,4]triazin-4(3H)-one

Colorless plates were obtained from the slow evaporation of a hexane/ ethyl acetate solution. Yield: 286 mg, 35%; mp 235-236 °C; ^{1}H NMR (400 MHz, DMSO) δ 9.02 (d, J = 5.5 Hz, 2H, pyridine), 8.06 (s, 2H, dichlorophenyl), 8.03 (s, 1H, dichlorophenyl), 7.86 (d, J = 5.4 Hz, 2H, pyridine), 7.83 (d, J = 8.3 Hz, 1H, benzimidazole), 7.56 (t, J = 7.7 Hz, 1H, benzimidazole), 7.40 (t, J = 7.7 Hz, 1H, benzimidazole), 6.63 (d, J = 8.5 Hz, 1H, benzimidazole). ^{13}C NMR (100 MHz, DMSO-*d*6) δ 151.22, 150.42, 144.00, 139.85, 137.71, 137.08, 134.45, 133.95, 133.41, 129.06, 126.78, 125.98, 124.06, 122.22, 120.69, 114.14. IR: 3030 (CH aromatic), 1691, 1630 (CON, C=N), 1598, 1575, 1547 (aromatic rings), 1442, 1434,1415, 1393, 1373, 1360, 1280, 1259, 1150, 1115, 840, 824, 811, 734 cm^{-1}; EI-LRMS *m/z* calcd. for $C_{20}H_{11}Cl_2N_5ONa$: [M+Na] = 430.02 found 430.02.

C4: 3-(2,4-difluorophenyl)-1-(pyridin-4-yl)benzo[4,5] imidazo[1,2-d][1,2,4]triazin-4(3H)-one

Colorless plates were obtained from the slow evaporation of a hexane/ ethyl acetate solution. Yield: 263 mg, 35%; mp 268-269 °C; ^{1}H NMR (400 MHz, DMSO-*d*6) δ 8.92

(d, J = 4.4 Hz, 2H, pyridine), 8.05 (d, J = 8.0 Hz, 1H, benzimidazole), 7.84 (d, J = 4.6 Hz, 2H, pyridine), 7.74 (dd, J = 14.5, 8.4 Hz, 1H, diflourophenyl), 7.60 (d, J = 4.5 Hz, 2H, pyridine), 7.56 (m, 2H, diflourophenyl), 7.40 (t, J = 7.8 Hz, 1H, benzimidazole), 7.31 (t, J = 7.1 Hz, 1H, benzimidazole), 6.63 (d, J = 8.4 Hz, 1H, benzimidazole). ^{13}C NMR (100 MHz, DMSO-*d*6) δ 164.03, 163.92, 163.81, 161.45, 161.33, 158.60, 158.47, 156.08, 155.94, 152.26, 151.11, 143.92, 141.12, 137.85, 137.12, 131.05, 130.94, 129.18, 126.70, 126.61, 124.72, 124.15, 122.16, 114.23, 112.96, 112.74, 105.71, 105.47, 105.20. IR: 3060 (CH aromatic), 1693, 1610 (CON, C=N), 1600, 1515 (aromatic rings), 1444, 1405, 1377, 1328, 1287, 1266, 1250, 1231, 1147, 994, 841, 809, 746, 734 cm^{-1}; EI-HRMS *m/z* calcd. for $C_{20}H_{11}F_2N_5ONa$: [M+Na] = 398.08304 found 398.08239.

Computational methodology

To investigate the potential inhibitory activity of the designed benzoimidazotriazinone derivatives against EGFR (Scheme 1), docking simulations were used to disclose if the designed compounds are amenable to fit within the ATP-binding site of the anticancer target with favorable interactions. EGFR is a member of the ErbB family of receptors, which includes EGFR (ErbB-1), HER2/c-neu (ErbB-2), HER3 (ErbB-3), and HER4 (ErbB-4). Mutations affecting EGFR expression or activity have been associated with several cancers, including lung and anal cancer (Zhang et al. 2007). The choice of the target emanated from the structural similarity between the proposed compounds and our previously designed EGFR inhibitors (Aliwaini et al. 2021a) and their structure–activity relationship requirements.

Docking experiment

The 2D chemical structure of the pyrazolotriazolopyrimidine derivatives (C1–4; Scheme 1) was sketched in Marvin Sketch (MarvinSketch16.10.24 2016) and saved in molfile format. Afterward, a group of energetically accessible conformers was generated using OMEGA software and saved in SDF format(OMEGA (Version 2.3.2) 2020). The X-ray crystal structure of EGFR (PDB ID: 4JRV; Resolution: 2.8 Å) (Peng et al. 2013) was obtained from Protein Data Bank (www.rcsb.

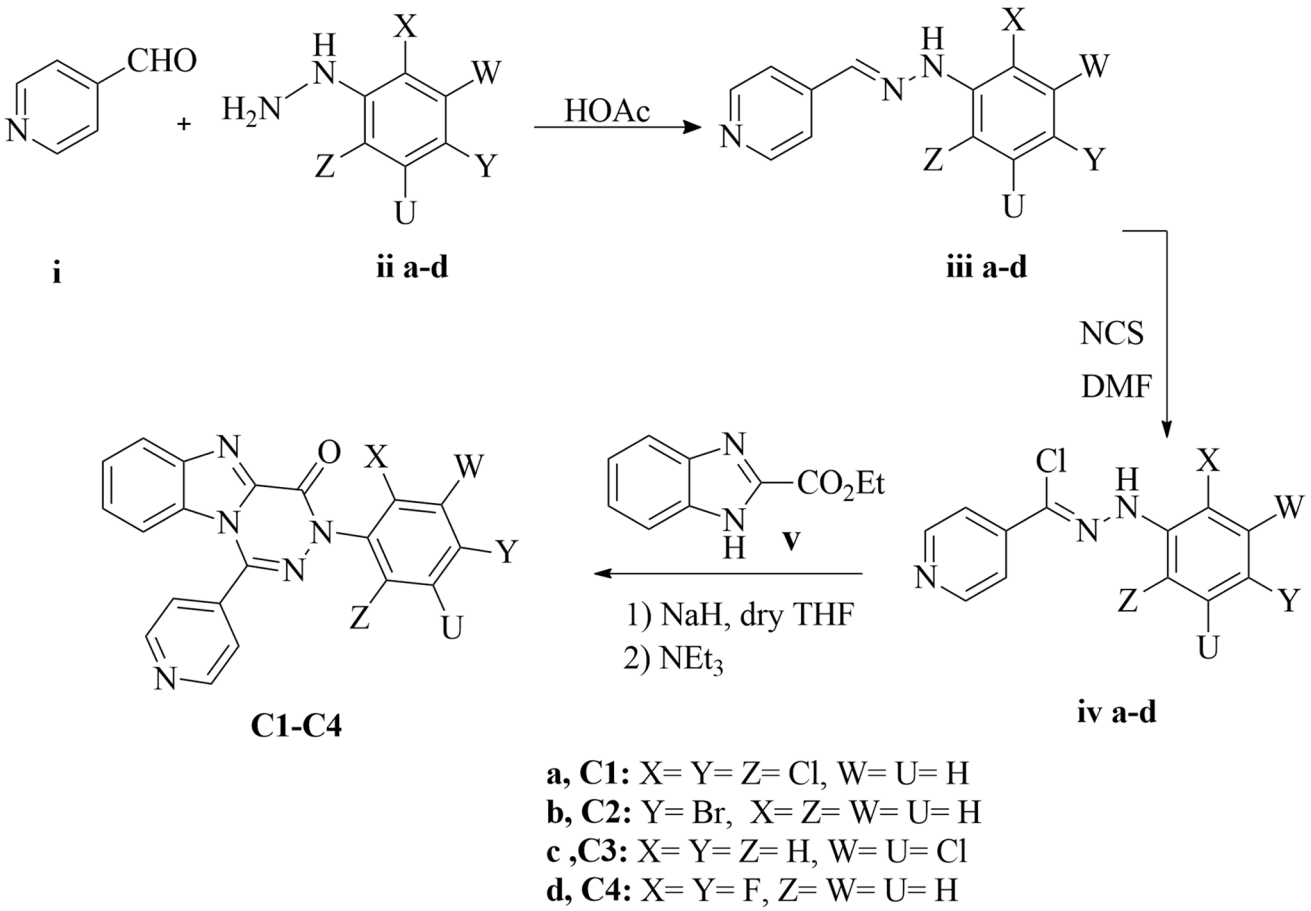

Scheme 1 Syntheses of the target compounds C1-C4

org). Hydrogen atoms were added to proteins using Discovery studio Visualizer templates for protein residues (DS visualizer 2022). The binding pocket with the outer contour was determined utilizing the pdb2 receptor protocol within OEDocking package software (OEDocking 2021). Subsequently, the ensemble of the generated conformers for the synthetic compounds was docked into the active site using FRED software. The protein structure and ligand conformers were treated as rigid throughout the docking process, which involved exhaustive scoring of all possible positions of ligands in the active binding site (OEDocking 2021). The top-scoring poses were optimized and assigned a final score.

Calculation of physicochemical properties

The drug-likeliness properties of the designed compounds were calculated using the molinspiration cheminformatics online software calculation toolkit, version 2018.10 (www.molinspiration.com).

Cell culture

Breast cancer cells HCC1937 and MCF7 cells were maintained in RPMI1640 supplemented with 10% FBS, 2 mM l-glutamine, 100 IU/Ml penicillin, and 100 µg/mL streptomycin. Cells were grown at 37°C in a humidified CO_2 incubator and subcultured every 3-5 days.

Determination of cell viability

Cell viability was determined by measuring the capacity of reducing enzymes present in viable cells to convert MTT to formazan crystals as described previously (Aliwaini et al. 2013). Briefly, cells were incubated with increasing concentrations of the synthesized compounds. After 48 h incubation, media were removed and 100 µL containing 1.2 mM MTT dissolved in PBS pH 7.4 was added to each well. After 4 h incubation at 37°C, the media were decanted by inverting the plate, and 100 µL of isopropyl alcohol was added to each well, with shaking for 1 h to dissolve the formazan crystals. The color intensity of the blue formazan solution formed in each well was measured at 570/690 nm using a BIO-TEK Instruments EL 312e microplate reader (Bio-Tek Instruments, Winooski, VT). The percentage of cell viability was calculated relative to vehicle-treated control designated as 100% viable cells.

Clonogenic survival assay

The clonogenic survival assay was performed to determine the long-term survival of both HCC1937 and MCF-7 cells after treatment with C3. Cells were seeded and treated with only the vehicle or C3. Twenty-four hours after treatment, cells were trypsinized, resuspended in fresh medium, and replated at a low density of 1000 cells per well in 6-well plates. Cells were grown and monitored for colony formation for 14 days. Media were routinely changed every 2 to 3 days. Surviving cells were washed with 1 X PBS, 3 times, fixed for 15 minutes in methanol: acetic acid (3:1) and excess fixative washed off with 1 X PBS, 3 times. Thereafter cells were stained for 15 minutes with 0.5% crystal violet (Sigma-Aldrich, USA) in 100% methanol (Aliwaini et al. 2021a). Colonies were imaged, and both size and number of colonies were quantified using ImageJ together with OriginPro 2021 software. The plating efficiency was calculated and presented ± SEM (Standard error of the means).

Growth curve assay

Breast cancer cells were seeded in triplicate in a 6-well plate and treated on the second day with C3 or vehicle. Cell numbers were assessed by counting after 24, 48 and 72 hours of treatment.

Scratch motility assay

Cells were grown to confluence and a linear wound was made through the monolayer using a sterile 200 µl pipette tip. To remove cell debris, the growth medium was replaced and several markings were made along the edges of the scratch line which were used as reference points. The wound widths were measured at the time of the scratching (0 hours) and after C3 treatment. Pictures were taken using an inverted light microscope (Olympus 1X71, USA) and a camera (Zeiss AxioCam, Germany). Migration distances were measured using Axiovert software (Zeiss, Germany). The difference in width represents the distance migrated in µm (Altaher et al. 2022).

Western blotting

Cells were harvested, and protein was prepared as described previously (Aliwaini et al. 2013). Primary antibodies used were: anti-EGFR, anti-pEGFR, anti-AKT, anti-pAKT, anti-PARP1/2 (sc-7150), anti-p53 (sc-126), anti-p21 (sc- 756) and anti-α-Tubulin (sc-8035) (Santa Cruz, California, USA).

Statistical analysis

Data presented are mean ± SEM of appropriate replicates. Statistical significance was assessed between the groups using the Student's t-test. A value of $P < 0.05$ was accepted as statistically significant.

Results

Synthesis of compounds

As shown in Scheme 1, compounds C1 to C4 were prepared via multistep reactions. 0.11 mol of different aryl hydrazines (II) were reacted with 0.1 mol of 4-pyridine carboxaldehyde (I) to obtain the corresponding hydrazones (III) as reported earlier (Abu Thaher et al. 2012d, a, 2016a, b; Wahedy et al. 2017; Aliwaini et al. 2021a). Then, the hydrazonyl chlorides (IV) were produced via a reaction of 0.011 mol of hydrazones with 0.012 mol of *N*-chlorosuccinimide (NCS) following the same procedure reported. After, the target compounds were prepared by deprotonation of 2.1 mmol of ethyl-2-benzimidazol carboxylate using 2.1 mmol of NaH in dry THF and 2 mmol of the corresponding pyridinecarbhydrazonoyl chloride (IV) was slowly added to the reaction mixture. This cycloaddition reaction was stirred overnight, and TLC monitored the progress of the reaction until completion. The products were purified by column chromatography. Structures of the novel target compounds were characterized and proved by spectroscopic methods, including ^{1}H-NMR, ^{13}C-NMR, IR and high-resolution mass spectra (HRMS). Finally, the X-Ray structures of compounds C1, C2 and C4 were previously determined (Abu Thaher et al. 2016a, b; Wahedy et al. 2017).

Molecular docking simulations

In order to explore the characteristic binding features of the synthesized compounds within the ATP-active site of EGFR, molecular docking simulations were carried out using FRED software [11]. The validation of FRED docking performance was conducted using re-docking (self-docking) to obtain the binding mode of the co-crystallized ligand within the active site of EGFR. FRED successfully predicted the positioning of the co-crystallized ligand with a lower root-mean-square deviation (RMSD) value. After validation, docking of the synthesized compounds C1–C4 was carried out, and the corresponding binding modes and binding energies were evaluated. Three out of the four docked compounds (C1-C3) were able to attain similar binding modes with favorable interactions with key amino acids similar to the co-crystallized ligand and complied with the SAR requirements of EGFR inhibitors. Fig. 2A shows the binding mode of the most active derivative (C1) within the active site of EGFR. At the molecular level, the binding modes of the designed compounds within the EGFR-binding site reveal multiple favorable interactions with key amino acid residues. Fig. 3 shows that the benzoimidazotriazinone ring forms hydrogen bonds with the hinge region connecting the *N*-terminal and C-terminal lobe of the kinase receptor. The nitrogen atom of the imidazole ring and/or carbonyl oxygen of the triazinone ring are in positions to form strong hydrogen bonds with the backbone amide NH of the key amino acid, Met769, in the active sites imilar to the co-crystallized inhibitor (Fig. 2D).

Furthermore, the pyridine *N* makes a water-bridged hydrogen bond with Asp776, while the aromatic pyridine ring makes a hydrophobic interaction with val702 (Fig. 3), similar to the co-crystallized ligand. Moreover, the halogen-substituted aromatic ring lies deep within a lipophilic pocket composed of Val702, Ala719, Lys721, Met742, Cys751, Leu764, Thr766 and Leu820 side chains and, thus, establishes predominantly hydrophobic interactions

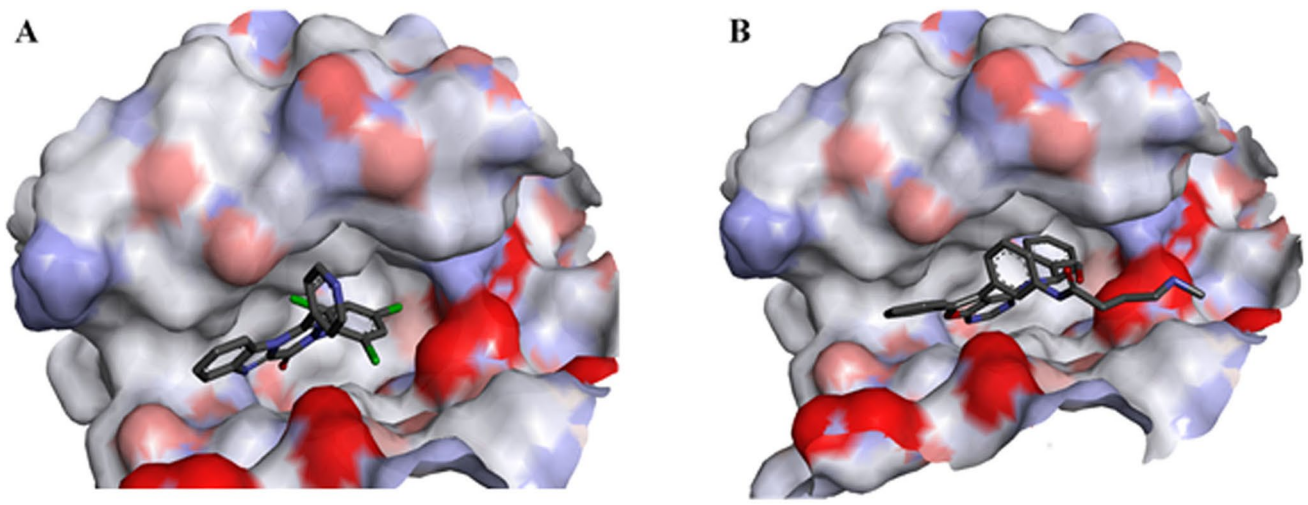

Fig. 2 **A** Solvent-accessible surface area of the binding site of EGFR crystal structure 4JRV (Rs = 2.8 Á) containing the docked pose of benzimidazotriazinone derivative (C1); **B** and the co-crystallized inhibitor (fuoropyrimidine derivative)

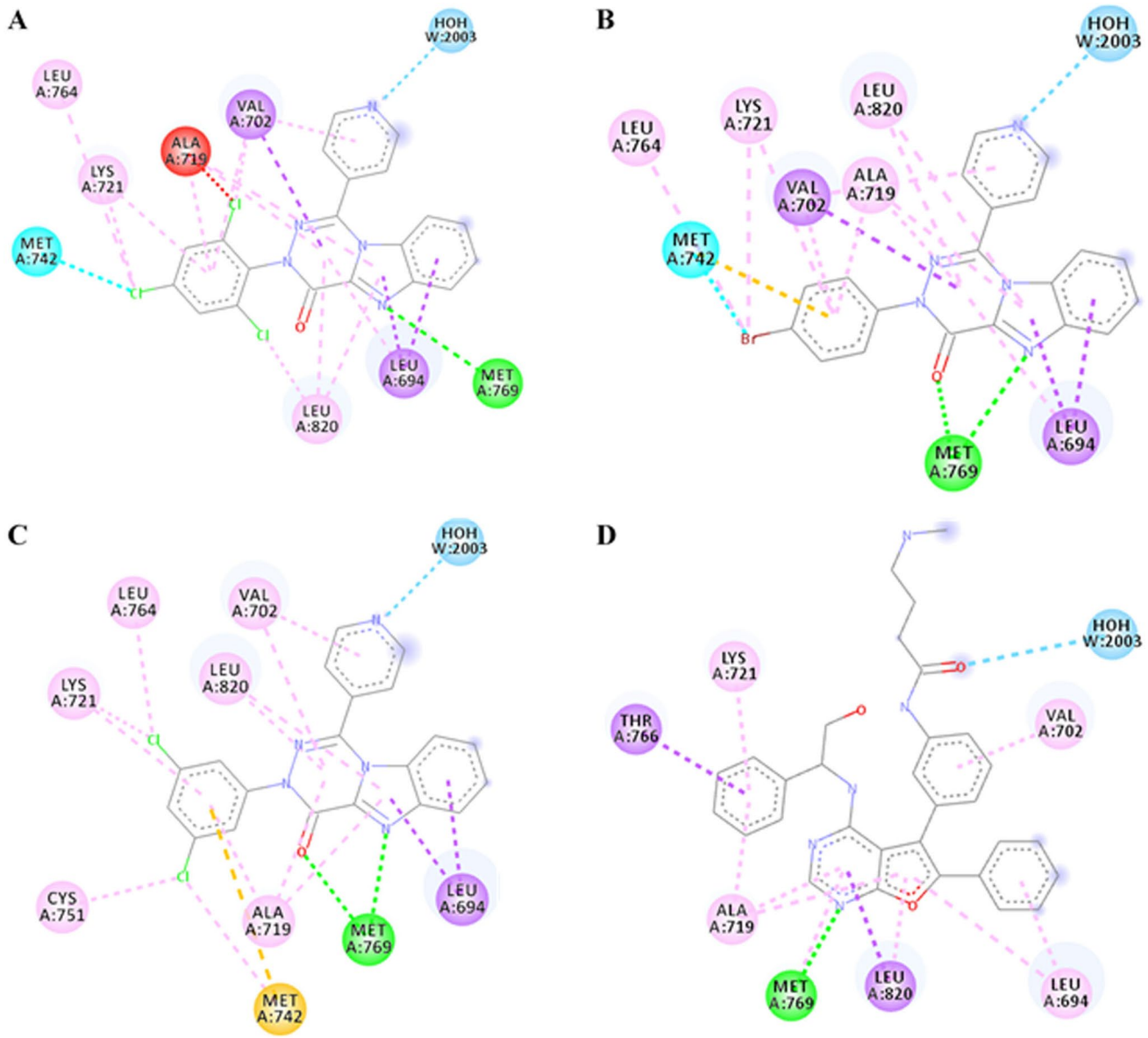

Fig. 3 2D binding diagram of pancreatic lipase amino acid residues interacting with: **A** C1; **B** C2; **C** C3 and **D** Co-crystallized inhibitor (furopyrimidine derivative)

with the target protein (Fig. 3). On the other hand, the tricyclic benzoimidazotriazinone ring is sandwiched between the side chains of Leu694, Val702, Ala 719, and Leu820, with possible van der Waals interactions. Each of these potential interactions contributes to the formation of stable ligand–EGFR complexes.

Table 1 Drug-likeliness prediction of the synthesized compounds using Molinspiration v2018.10. PSA: polar surface area; NRB: number of rotatable bonds; miLog*P*: Log partition coefficient; HBA: number of hydrogen bond acceptors; HBD: number of hydrogen bond donors; Mol Vol: molecular volume; MW: molecular weight; %ABS: percentage absorption

Compound	PSA	NRB	miLogP	HBA	HBD	Mol Vol	MW	%ABS
C1	65.10	2	5.30	6	0	332.70	442.69	86.54%
C2	65.10	2	3.79	6	0	309.98	418.25	86.54%
C3	65.10	2	4.69	6	0	319.16	408.25	86.54%
C4	65.10	2	3.45	6	0	301.95	375.34	86.54%

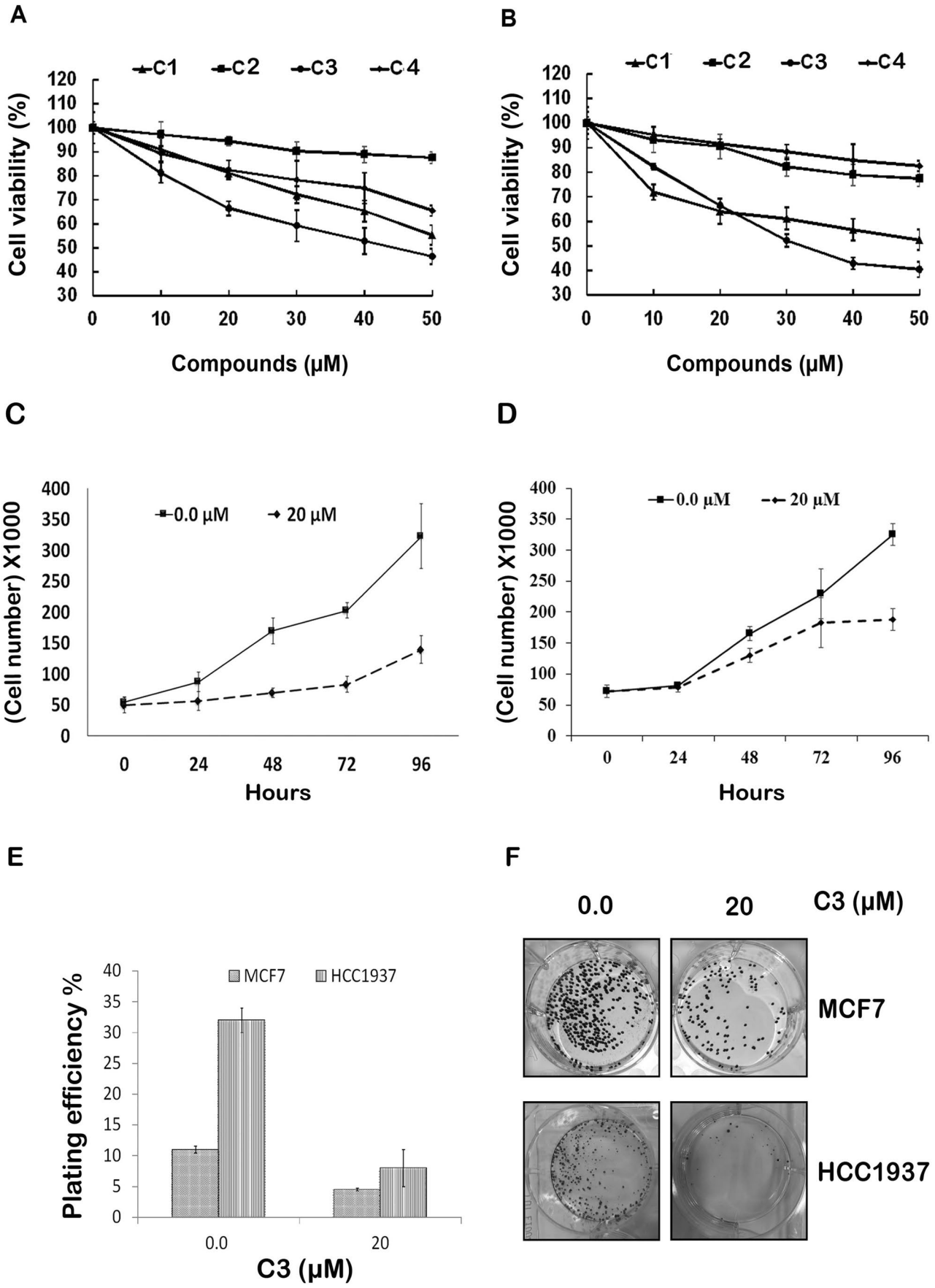
A
C1
C2
C3
C4
Cell viability (%)
Compounds (μM)
B
C1
C2
C3
C4
Cell viability (%)
Compounds (μM)
C
0.0 μM
20 μM
(Cell number) X1000
Hours
D
0.0 μM
20 μM
(Cell number) X1000
Hours
E
MCF7
HCC1937
Plating efficiency %
C3 (μM)
F
0.0
20
C3 (μM)
MCF7
HCC1937

◂**Fig. 4** Anti-growth effect of different compounds (C1 to C4) against MCF7 HCC1937 breast cancer cells. **A** and **b** Cell viability was tested using the MTT assay, and data were expressed as a percentage of vehicle-treated control ± SEM. **C** and **D** The curves of MCF7 (**A**) and HCC1937 (**B**) breast cancer cell lines treated with the vehicle or 20 µM of C3.The difference was significant after the sixth day ($P<0.05$). **E** and **F** Anti-colony formation effect of C3 against MCF7 and HCC1937 cells. **E** C3 reduces the plating efficiency of both cell lines. **F** Representative images of clonogenic results for MCF7 and HCC1937 cells treated with vehicle or 20 µM of C3

Calculation of molecular properties and drug-likeliness

To be an effective drug, a sufficient amount of a potent molecule must reach its target. Therefore, good oral bioavailability is often an essential requirement in the discovery and development of drugs. Thus, it is very important in drug design to consider the physicochemical properties that increase oral bioavailability. Several rules were suggested to predict drug-likeliness. The most common approach is Lipinski's rule of five. However, other researchers have proposed other approaches, namely Veber, Egan, Muegge, and Ghoose (Loureiro et al. 2019). Lipinski's Rule of Five is commonly utilized to predict the bioavailability of active leads. Thus, different *in silico* computational methods that predict ADME parameters from molecular descriptors were utilized. Herein, we adopted a Molinspiration cheminformatics online software calculation toolkit to obtain Lipinski's parameters and polar surface area (PSA) of the synthesized compounds. The absorption percentage (%ABS) was calculated by using the following formula: $\%ABS = 109 - 0.345 \times PSA$ (Zhao et al. 2002). According to Lipinski's Rule of Five, a potential lead will likely be orally active if the molecule satisfies the following: (i) molecular weight (MW) ≤500, (ii) number of hydrogen bond donors (OH and NH groups) ≤5, (iii) number of hydrogen bond acceptors (notably N and O) ≤10, and (iv) calculated octanol/water partition coefficient (Log *P*) ≤5. Molecules violating more than one of these rules may lead to inadequate bioavailability (Table 1)(Zhao et al. 2002). The results in Table 1 revealed that the four designed molecules (C1, C2, C3 and C4) fulfill Lipinski's Rule of Five with the exception of one C-1 violation1 (Log*P* >5). Two other descriptors were identified by Veber et al. (2002): the numbers of rotatable bonds are (NRB) ≤10 and PSA <140 $Å^2$ (Veber et al. 2002). Overall, the four compounds largely met the Lipinski and Veber Rules, suggesting that these compounds theoretically have good oral bioavailability. Finally, the calculated percentage of absorption for each derivative was 86.54%, indicating that they may have good cell membrane permeability.

Antiproliferative effects of the synthesized compounds

To determine the antiproliferative capacity of the compounds C1 to C4, two breast cancer cell lines MCF7 and HCC1937 cells were plated and treated with different concentrations of the compounds for 48 h, and cell proliferation was determined using the MTT assay. As shown in Fig. 4, the most active compound was C3, which showed the most potent cytotoxic effect on cell viability with an IC_{50} of 36.4 and 48.2 µM against both MCF7 and HCC1937 cells, respectively. The other three compounds showed lower cytotoxic effects than C3 with IC_{50s} more than 40 µM against both breast cancer cell lines. The small molecule EGFR inhibitor (CAS 879127-07-8) was used as a positive control and showed a potent anti-proliferative effect with IC_{50} of 5.4 and 2.96 µM against HCC1937 and MCF7 cells, respectively. Fig. 4C-D shows that C3 significantly reduces the growth rate of both tested cell lines. C3 significantly inhibited colony formation in both MCF-7 and HCC1937 cells (Fig. 4E-F).

C3 inhibits the migration of human breast cancer cells

A scratch motility assay was performed to explore the anti-migration ability of C3. A significant decrease in cell migration was observed for both cell lines exposed to 20 µM C3 for 48, 72 and 96 hours (Fig. 5A, B and C). Taken together, these data demonstrate that C3 has an anti-migratory effect on both MCF7 and HCC1937 breast cancer cells.

C3 inhibits EGFR signaling and induces cell cycle arrest and apoptosis in breast cancer cells

To understand the molecular mechanism behind the C3 cytotoxic effect, the possible impact on EGFR signaling, cell cycle progression and apoptosis was investigated. Data demonstrated that C-3 treatment decreased p-EGFR level and its downstream targets p-AKT in both MCF and HCC1937 cells (Fig. 6). Furthermore, Fig. 6 indicates that both breast cancer cells showed a clear increase in p53 and p21 levels after 48 hours of treatment. Importantly, cleaved PARP, an apoptotic marker, was also increased significantly after 48 hours of C3 treatment. In accordance with these results, previous reports demonstrated that inhibition of EGFR by synthetic pyrazolo-[4,3-e][1,2,4]triazolopyrimidine derivatives, erlotinib, gefitinib, cetuximab or panitumumab lead to G1 cell cycle arrest and apoptosis (Aliwaini et al. 2021b). These observations indicate that C3 inhibits EGFR signaling and induces cell cycle arrest and apoptosis in MCF7 and HCC1937.

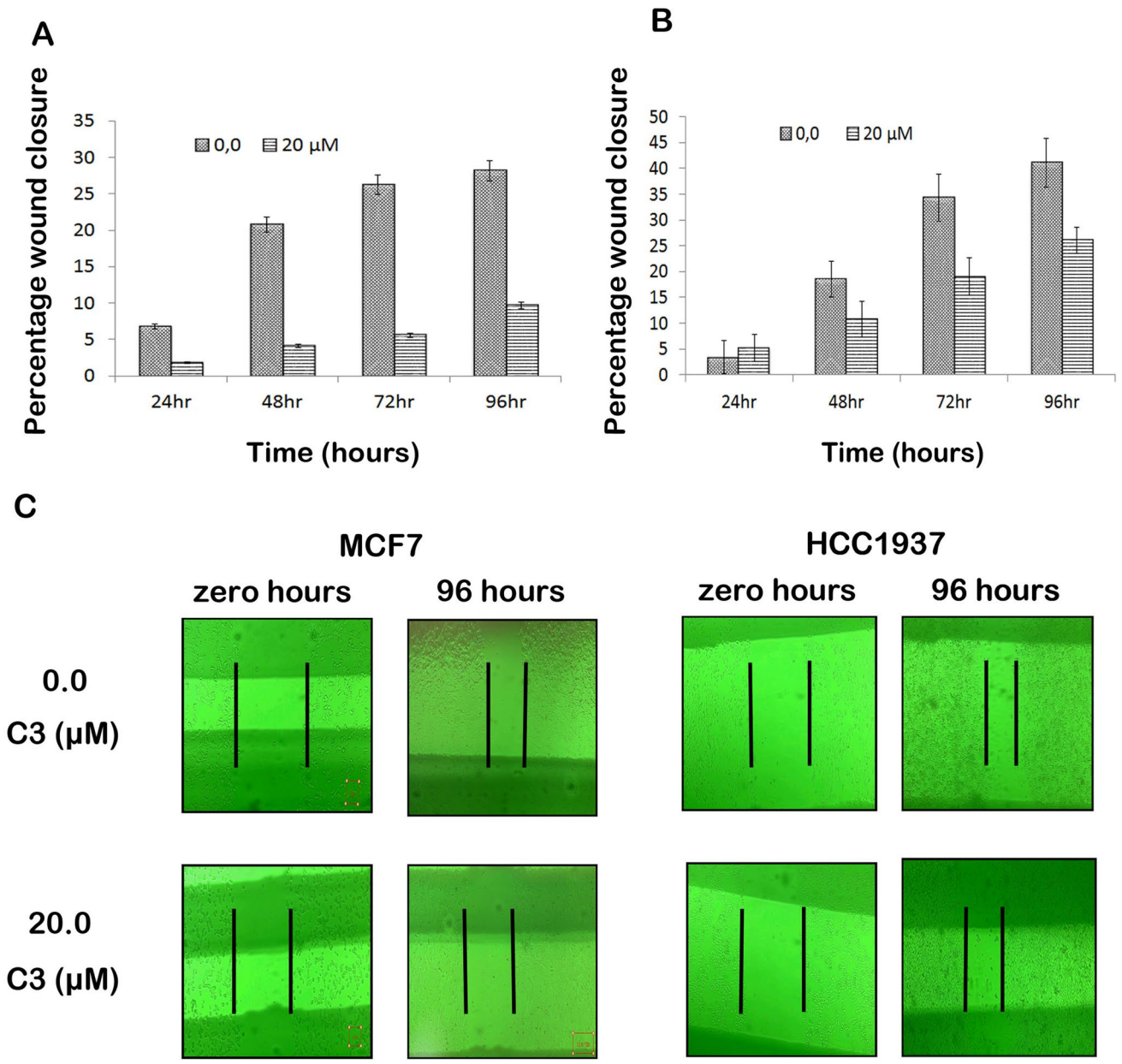

Fig. 5 C3 inhibits the migration of breast cancer cells. **A** and **B** graphs show the ability of C-3 to inhibit the migratory ability of MCF7 and HCC1937 breast cancer cells, respectively. **C** At specified time points (0 and 96 hours) cells were photographed using 10x; magnification (Olympus 1X71). Assays were carried out in duplicate, and two independent experiments were performed

Discussion

Cancer is one of the leading causes of death worldwide. Despite the significant progress in cancer therapies, the number of cancer deaths is expected to elevate to 13.5 million deaths in 2030 (Siegel et al. 2020). The major disadvantages of current treatments are low specificity, resulting in unwanted side effects, and drug resistance (Seifert 2019). Thus, there is an urgent demand to develop novel anticancer therapeutics. Triazines, a family of heterocyclic aromatic compounds containing three nitrogen atoms, exist in three isomeric forms, 1,2,3-triazine, 1,2,4-triazine, and 1,3,5-triazine, based on the position of the nitrogen atoms (Kushwaha and Sharma 2020). They exhibit potent antitumor effects by interacting with several targets in cancer cells, which interfere with important signaling pathways to induce cell cycle arrest and apoptosis (Peterson et al. 2011; Schuler et al. 2020; Majeed Ganai et al.

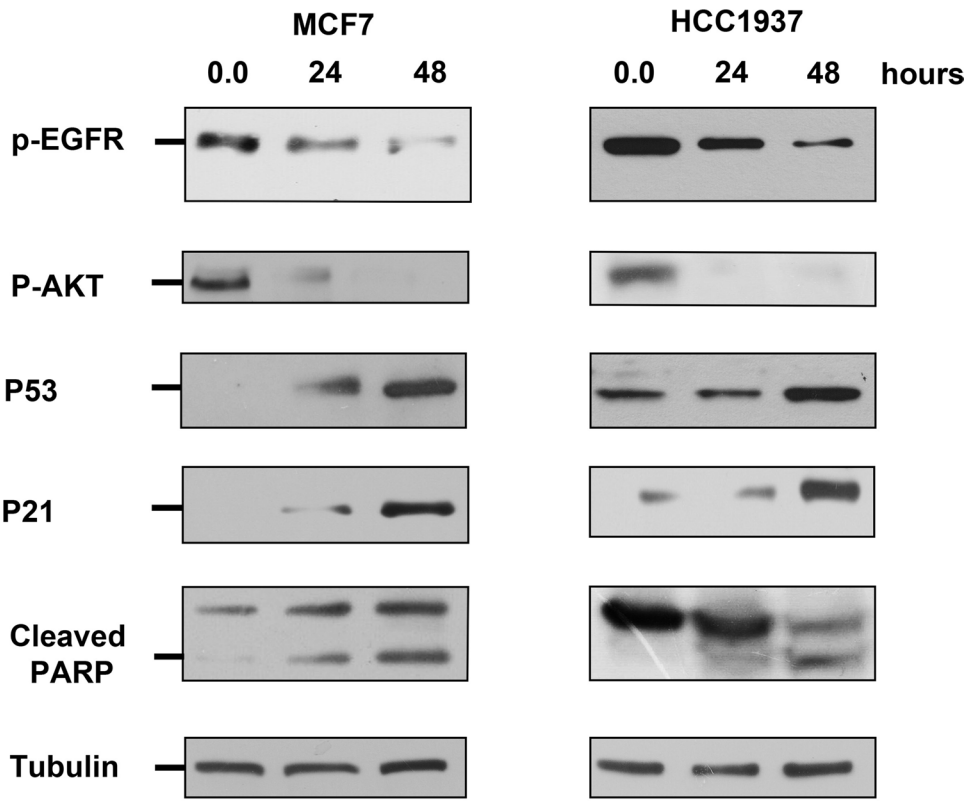

Fig. 6 C3 inhibits EGFR signaling and induces cell cycle arrest and apoptosis in MCF7 and HCC1937 breast cancer cells. Western blotting of proteins from the indicated cancer cells treated with 20 μM of C3 for 24 and 48 hours and analyzed with antibodies to p-EGFR, p-AKT, p53, p21, and cleaved PARP. Tubulin was used as a loading control

2021; Hashem et al. 2022). To date, many triazine hybrids including avapritinib, brivanib, capmatinib, tretamine, HL 010183, gedatolisib, and enasidenib are already approved to treat lung, cervical, hepatocellular, and metastatic breast cancer indications (Schuler et al. 2020; Liang et al. 2021; Hashem et al. 2022; Dong et al. 2022). The encouraging precedent of capmatinib has led us to develop a new molecular system by exchanging the imidazole ring with benzimidazole moiety to increase the lipophilicity of the compound and its penetration through the cell membrane. Four new 3-Aryl -1-(pyridin-4-yl)benzo[4,5]imidazo[1,2-*d*][1,2,4]- triazin-4(*3H*)-ones derivatives (C1 to C4) were prepared, characterized and verified by spectroscopic methods, including ^{1}H-NMR, ^{13}C-NMR, IR, X-ray analysis and high-resolution mass spectra (HRMS). ^{1}H-NMR of all target compounds showed the disappearance of NH and OCH_2CH_3 protons of ethyl-2-benzimidazole carboxylate. Where the loss of these six protons confirms its cyclization with the corresponding nitrilimine to afford the fused rings of Benzoimidazo[1,2,4] triazinones. Furthermore, ^{13}C-NMR showed a loss of OCH_2CH_3 carbons of the benzimidazole ester which confirms the same result that agreed with the evaluated molecular masses of the cyclized target compounds. In addition, all the IR spectra exhibited the absence of the NH band of benzimidazole moiety as significant evidence for the cyclization process.

Biologically, the compounds displayed different levels of cytotoxicity against the triple negative HCC1937, and the estrogen receptor positive MCF7 breast cancer cells. C3 exhibited the most potent antiproliferative effect against both MCF7 and HCC1937 breast cancer cell lines with IC_{50} values of 36.4 and 48.2 μM. Importantly, C3 inhibited EGFR signaling and induced cell cycle arrest and apoptosis as indicated by the low levels of p-EGFR and p-AKT and the increasing levels of p53, p21 and cleaved PARP. A recent study describing the synthesis and anticancer activities of a new benzimidazole series, 1,2,4-triazoles and 1,3,5-triazine showed similar findings (Hashem et al. 2022). Three of these compounds showed potent antiproliferative effects against lung and breast cancer cells with an IC50 range of 2.5-60.0 μM. Importantly, these compounds demonstrated potent suppression activity against both wild-type and mutated EGFR in addition to increased p53 levels. An earlier study identified a group of triazine benzimidazoles that inhibit the PI3K/AKT/mTOR pathway (Stec et al. 2015). Compound 18 of that group showed a significant *in vivo* inhibition of AKT phosphorylation at all doses evaluated in the study. These observations are consistent with our results in which C3 inhibited the p-EGFR and p-AKT levels in both breast cancer cells.

Inhibition of EGFR abolishes its downstream signaling pathways, such as phosphatidylinositol 3 kinase pathway

PI3K/AKT/mTOR. This pathway is one of the main signaling pathways regulated by EGFR and plays a critical role in cancer development (Jung et al. 2021). Phosphorylation of EGFR at site Y1068 causes activation of AKT at site s473 (Sette et al. 2015). Our data show that C3 inhibits this pathway by inhibition of AKT phosphorylation at site s473 site in a time-dependent manner. Activating mutations of AKT indirectly down-regulate p53 levels by enhancing MDM2 protein, which is known to mediate p53 degradation. Thus, inhibition of AKT phosphorylation leads to the prevention of p53 from degradation (Abraham and O'Neill 2014). As a confirmation, our data also show that C-3 increases p21, an established target of p53.

Conclusion

Taken together, it has been investigated that C3 is a new potent antitumor agent exhibiting a promising inhibitory impact against the EGFR signaling pathway. These advantages together indicate that C3 is a worthwhile lead compound for the development of new, more potent anticancer drugs inhibiting the EGFR pathway.

Acknowledgments Bassam Abu Thaher would like to thank by the Palestinian Research Council (Ramallah) for funding and Alexander von Humboldt Foundation (AvH) for funding his short visit, in 2022.

Authors' contributions B.A, B.Q and R.M prepared the compounds. C.J and H.D supervised the chemical design and synthesis. I. A and K.W performed the modeling. S.I wrote the main manuscript and supervised the biological work.S.kh, I.A, A.M, and A. I performed biological experiments. All authors reviewed the manuscript. The authors declare that all data were generated in-house and that no paper mill was used

Funding This work was supported by Palestinian Research Council (Ramallah) and Alexander von Humboldt Foundation (AvH) for funding his short visit, in 2022.

Availability of data and materials The original contributions presented in the study are included in the article, and further inquiries can be directed to the corresponding author.

Declarations

Ethical approval Not applicable.

Competing interests The authors declare no financial AND non-financial interests conflict of interest.

References

AboulWafa OM, Daabees HMG, Badawi WA (2020) 2-Anilinopyrimidine derivatives: Design, synthesis, in vitro anti-proliferative activity, EGFR and ARO inhibitory activity, cell cycle analysis and molecular docking study. Bioorg Chem 99:103798. https://doi.org/10.1016/j.bioorg.2020.103798

Abraham AG, O'Neill E (2014) PI3K/Akt-mediated regulation of p53 in cancer. Biochem Soc Trans 42:798–803. https://doi.org/10.1042/BST20140070

Abu Thaher B, Koch P, Schollmeyer D, Laufer S (2012) Ethyl 5-amino-3-(pyridin-4-yl)-1-(2,4,6-tri-chlorophenyl)-1H-pyrazole-4- carboxylate dimethyl sulfoxide hemisolvate. Acta Crystallogr Sect E Struct Reports Online 68:o917-8. https://doi.org/10.1107/S1600536812008264

Abu Thaher B, Koch P, Schollmeyer D, Laufer S (2012) 4-(4-Fluorophenyl)-1-(4-nitrophenyl)-3-(pyridin-4-yl)-1H-pyrazol-5-amine. Acta Crystallogr Sect E Struct Reports Online 68:o633. https://doi.org/10.1107/S1600536812004102

Abu Thaher B, Koch P, Schollmeyer D, Laufer S (2012) 4-(4-Fluorophenyl)-3-(pyridin-4-yl)-1-(2,4,6-trichlorophenyl) -1H-pyrazol-5-amine. Acta Crystallogr Sect E Struct Reports Online 68:o2603. https://doi.org/10.1107/S1600536812033569

Abu Thaher B, Koch P, Schollmeyer D, Laufer S (2012) 4-(4-Fluorophenyl)-1-phenyl-3-(pyridin-4-yl)-1H-pyrazol-5-amine. Acta Crystallogr Sect E Struct Reports Online 68:o632. https://doi.org/10.1107/S1600536812004096

Abu Thaher B, Schollmeyer D, Qeshta B, Deigner H-P (2016a) 3-(2,4-Difluorophenyl)-1-(pyridin-4-yl)benzo[4,5]imidazo[1,2-d][1,2,4]triazin-4(3 H)-one . IUCrData 1:x161380-. https://doi.org/10.1107/S2414314616013808/HB4075ISUP3.CML

Abu Thaher B, Schollmeyer D, Qeshta B, Deigner H-P (2016b) 3-(2,4-Difluorophenyl)-1-(pyridin-4-yl)benzo[4,5]imidazo[1,2- d][1,2,4]triazin-4(3 H)-one . IUCrData 1:. https://doi.org/10.1107/S2414314616013808

Akhtar MJ, Khan AA, Ali Z et al (2018) Synthesis of stable benzimidazole derivatives bearing pyrazole as anticancer and EGFR receptor inhibitors. Bioorg Chem 78:158–169. https://doi.org/10.1016/j.bioorg.2018.03.002

Aliwaini S, Swarts AJAJAJ, Blanckenberg A et al (2013) A novel binuclear palladacycle complex inhibits melanoma growth in vitro and in vivo through apoptosis and autophagy. Biochem Pharmacol 86:1650–1662. https://doi.org/10.1016/j.bcp.2013.09.020

Aliwaini S, Thaher BA, Al-masri I et al (2021) Design, synthesis and biological evaluation of novel pyrazolo[1,2,4]triazolopyrimidine derivatives as potential anticancer agents. Molecules 26:4065. https://doi.org/10.3390/molecules26134065

Aliwaini S, Thaher BA, Al-masri I et al (2021) Design, Synthesis and Biological Evaluation of Novel Pyrazolo[1,2,4]triazolopyrimidine Derivatives as Potential Anticancer Agents. Mol 26:4065. https://doi.org/10.3390/MOLECULES26134065

Altaher A, Adris M, Aliwaini S et al (2022) The Anticancer Effects of Novel Imidazo[1,2-a]Pyridine Compounds against HCC1937 Breast Cancer Cells. Asian Pacific J Cancer Prev 23:2943–2951. https://doi.org/10.31557/apjcp.2022.23.9.2943

Burnet MW, Thaher BA, Jan Ehlert Kubbutat M, Schaechtele C, Totzke F (2016) (12) United States Patent. 2:1–28

Celik İ, Ayhan-Kılcıgil G, Guven B et al (2019) Design, synthesis and docking studies of benzimidazole derivatives as potential EGFR inhibitors. Eur J Med Chem 173:240–249. https://doi.org/10.1016/j.ejmech.2019.04.012

Choi W, Park SY, Lee Y et al (2021) The Clinical Impact of Capmatinib in the Treatment of Advanced Non-Small Cell Lung Cancer with MET Exon 14 Skipping Mutation or Gene Amplification. Cancer Res Treat 53:1024–1032. https://doi.org/10.4143/crt.2020.1331

Dong G, Jiang Y, Zhang F et al (2022) Recent updates on 1,2,3-, 1,2,4-, and 1,3,5-triazine hybrids (2017–present): The anticancer activity,

structure–activity relationships, and mechanisms of action. Arch Pharm (Weinheim). https://doi.org/10.1002/ardp.202200479
DS visualizer (2022) Accelrys Discovery Studio Visualizer 3.0 Download (Free) - DiscoveryStudio25.exe. https://accelrys-discovery-studio-visualizer.software.informer.com/3.0/. Accessed 24 Mar 2020
Gaber AA, Bayoumi AH, El-morsy AM et al (2018) Design, synthesis and anticancer evaluation of 1H-pyrazolo[3,4-d]pyrimidine derivatives as potent EGFR WT and EGFR T790M inhibitors and apoptosis inducers. Bioorg Chem 80:375–395. https://doi.org/10.1016/j.bioorg.2018.06.017
Gellis A, Kovacic H, Boufatah N, Vanelle P (2008) Synthesis and cytotoxicity evaluation of some benzimidazole-4,7-diones as bioreductive anticancer agents. Eur J Med Chem 43:1858–1864. https://doi.org/10.1016/J.EJMECH.2007.11.020
Guo H, Diao Q-P (2020) 1,3,5-Triazine-azole Hybrids and their Anticancer Activity. Curr Top Med Chem 20:1481–1492. https://doi.org/10.2174/1568026620666200310122741
Hashem HE, Amr AEGE, Nossier ES et al (2022) New Benzimidazole-, 1,2,4-Triazole-, and 1,3,5-Triazine-Based Derivatives as Potential EGFRWTand EGFRT790MInhibitors: Microwave-Assisted Synthesis, Anticancer Evaluation, and Molecular Docking Study. ACS Omega 7:7155–7171. https://doi.org/10.1021/acsomega.1c06836
Jung S, Kim DH, Choi YJ et al (2021) Contribution of p53 in sensitivity to EGFR tyrosine kinase inhibitors in non-small cell lung cancer. Sci Rep 11:1–10. https://doi.org/10.1038/s41598-021-99267-z
Kayki G, Zinnet M, Aksoyalp S et al (2022) A year in pharmacology : new drugs approved by the US Food and Drug Administration in 2021. Naunyn Schmiedebergs Arch Pharmacol 395:867–885. https://doi.org/10.1007/s00210-022-02250-2
Krause M, Foks H, Gobis K (2017) Pharmacological potential and synthetic approaches of imidazo[4,5-b]pyridine and imidazo[4,5-c]pyridine derivatives. Molecules 22:399. https://doi.org/10.3390/molecules22030399
Kushwaha N, Sharma CS (2020) The Chemistry of Triazine Isomers: Structures, Reactions, Synthesis and Applications. Mini-Reviews Med Chem 20:2104–2122. https://doi.org/10.2174/1389557520666200729160720
Liang Q, Wang J, Zhao L et al (2021) Recent advances of dual FGFR inhibitors as a novel therapy for cancer. Eur J Med Chem 214:113205. https://doi.org/10.1016/j.ejmech.2021.113205
Loureiro DRP, Soares JX, Costa JC et al (2019) Structures, Activities and Drug-Likeness of Anti-Infective Xanthone Derivatives Isolated from the Marine Environment: A Review. Mol 24:243. https://doi.org/10.3390/MOLECULES24020243
Majeed Ganai A, Khan Pathan T, Hampannavar GA et al (2021) Recent Advances on the s-Triazine Scaffold with Emphasis on Synthesis, Structure-Activity and Pharmacological Aspects: A Concise Review. ChemistrySelect 6:1616–1660. https://doi.org/10.1002/slct.202004591
MarvinSketch16.10.24 (2016) ChemAxon - Software Solutions and Services for Chemistry & Biology
Nawaz F, Alam O, Perwez A et al (2020) 3′-(4-(Benzyloxy)phenyl)-1′-phenyl-5-(heteroaryl/aryl)-3,4-dihydro-1′H,2H-[3,4′-bipyrazole]-2-carboxamides as EGFR kinase inhibitors: Synthesis, anticancer evaluation, and molecular docking studies. Arch Pharm (Weinheim) 353:1900262. https://doi.org/10.1002/ardp.201900262
OEDocking (2021) OEDocking Software | Molecular Docking Tools | Fred Docking. https://www.eyesopen.com/oedocking. Accessed 24 Mar 2020
OMEGA (Version 2.3.2) (2020) OMEGA 4.2.1.2: OpenEye Scientific Software, Santa Fe. https://www.eyesopen.com
Peng YH, Shiao HY, Tu CH et al (2013) Protein kinase inhibitor design by targeting the Asp-Phe-Gly (DFG) motif: The role of the DFG motif in the design of epidermal growth factor receptor inhibitors. J Med Chem 56:3889–3903
Peterson EA, Andrews PS, Be X et al (2011) Discovery of triazine-benzimidazoles as selective inhibitors of mTOR. Bioorganic Med Chem Lett 21:2064–2070. https://doi.org/10.1016/j.bmcl.2011.02.007
Refaat HM (2010) Synthesis and anticancer activity of some novel 2-substituted benzimidazole derivatives. Eur J Med Chem 45:2949–2956. https://doi.org/10.1016/J.EJMECH.2010.03.022
Sahin Z, Biltekin SN, Ozansoy M et al (2022) Synthesis and in vitro antitumor activities of novel thioamide substituted piperazinyl-1,2,4-triazines. J Heterocycl Chem 59:1333–1340. https://doi.org/10.1002/jhet.4470
Schuler M, Berardi R, Lim WT et al (2020) Molecular correlates of response to capmatinib in advanced non-small-cell lung cancer: clinical and biomarker results from a phase I trial. Ann Oncol 31:789–797. https://doi.org/10.1016/j.annonc.2020.03.293
Seifert R (2019) Basic Knowledge of Pharmacology
Sette G, Salvati V, Mottolese M et al (2015) Tyr1068-phosphorylated epidermal growth factor receptor (EGFR) predicts cancer stem cell targeting by erlotinib in preclinical models of wild-type EGFR lung cancer. Cell Death Dis 6:e1850. https://doi.org/10.1038/cddis.2015.217
Sharma P, Larosa C, Antwi J et al (2021) Imidazoles as potential anticancer agents: An update on recent studies. Molecules 26:4213. https://doi.org/10.3390/molecules26144213
Sherbiny FF, Bayoumi AH, El-Morsy AM et al (2021) Design, Synthesis, biological Evaluation, and molecular docking studies of novel Pyrazolo[3,4-d]Pyrimidine derivative scaffolds as potent EGFR inhibitors and cell apoptosis inducers. Bioorg Chem 116:105325. https://doi.org/10.1016/j.bioorg.2021.105325
Siegel RL, Miller KD, Jemal A (2020) Cancer statistics, 2020. CA Cancer J Clin 70:7–30. https://doi.org/10.3322/caac.21590
Singla P, Luxami V, Paul K (2015) Triazine-benzimidazole hybrids: Anticancer activity, DNA interaction and dihydrofolate reductase inhibitors. Bioorganic Med Chem 23:1691–1700. https://doi.org/10.1016/j.bmc.2015.03.012
Sivaramakarthikeyan R, Iniyaval S, Saravanan V et al (2020) Molecular Hybrids Integrated with Benzimidazole and Pyrazole Structural Motifs: Design, Synthesis, Biological Evaluation, and Molecular Docking Studies. ACS Omega 5:10089–10098. https://doi.org/10.1021/acsomega.0c00630
Stec MM, Andrews KL, Bo Y et al (2015) The imidazo[1,2-a]pyridine ring system as a scaffold for potent dual phosphoinositide-3-kinase (PI3K)/mammalian target of rapamycin (mTOR) inhibitors. Bioorganic Med Chem Lett 25:4136–4142. https://doi.org/10.1016/j.bmcl.2015.08.016
Tan L, Zhang J, Wang Y et al (2022) Development of Dual Inhibitors Targeting Epidermal Growth Factor Receptor in Cancer Therapy. J Med Chem 65:5149–5183. https://doi.org/10.1021/ACS.JMEDCHEM.1C01714/ASSET/IMAGES/MEDIUM/JM1C01714_0024.GIF
Thaher BA, Arnsmann M, Totzke F et al (2012) Tri- and tetrasubstituted pyrazole derivates: Regioisomerism switches activity from p38MAP kinase to important cancer kinases. J Med Chem 55:961–965. https://doi.org/10.1021/JM201391U/SUPPL_FILE/JM201391U_SI_001.PDF
Thomas HD, Calabrese CR, Batey MA et al (2007) Preclinical selection of a novel poly(ADP-ribose) polymerase inhibitor for clinical trial. Mol Cancer Ther 6:945–956. https://doi.org/10.1158/1535-7163.MCT-06-0552
Veber DF, Johnson SR, Cheng HY et al (2002) Molecular properties that influence the oral bioavailability of drug candidates. J

Med Chem 45:2615–2623. https://doi.org/10.1021/JM020017N/SUPPL_FILE/JM020017N_S.PDF

Wahedy K, Thaher BA, Schollmeyer D et al (2017) Crystal structures of pure 3-(4-bromo-2-chlorophenyl)-1-(pyridin-4-yl)benzo[4,5]imidazo-[1,2-d][1,2,4]triazin-4(3H)-one and contaminated with 3-(4-bromophenyl)-1-(pyridin-4-yl)benzo-[4,5]imidazo[1,2-d][1,2,4]triazin-4(3H)-one. Acta Crystallogr Sect E Crystallogr Commun 73:1341–1343

Yuan X, Yang Q, Liu T et al (2019) Design, synthesis and in vitro evaluation of 6-amide-2-aryl benzoxazole/benzimidazole derivatives against tumor cells by inhibiting VEGFR-2 kinase. Eur J Med Chem 179:147–165. https://doi.org/10.1016/j.ejmech.2019.06.054

Zhang H, Berezov A, Wang Q et al (2007) Review series ErbB receptors : from oncogenes to targeted cancer therapies. Molecules 117:2051–2058. https://doi.org/10.1172/JCI32278.The

Zhang J, Che J, Luo X et al (2022) Structural Feature Analyzation Strategies toward Discovery of Orally Bioavailable PROTACs of Bruton's Tyrosine Kinase for the Treatment of Lymphoma. J Med Chem 65:9096–125. https://doi.org/10.1021/acs.jmedchem.2c00324

Zhao YH, Abraham MH, Le J et al (2002) (2002) Rate-Limited Steps of Human Oral Absorption and QSAR Studies. Pharm Res 1910(19):1446–1457. https://doi.org/10.1023/A:1020444330011